Digital image compression for a 2f multiplexing optical setup

J Vargas[1,2], D Amaya[1,3,4] and E Rueda[1]

[1] Grupo de Óptica y Fotónica, Instituto de Física, Facultad de Ciencias Exactas y Naturales, Universidad de Antioquia U de A, Calle 70 No. 52-21, Medellín, Colombia
[2] Instituto Tecnológico Metropolitano, Calle 73 No 76A-354. AA 54959. Medellín, Colombia
[3] Centro de Investigaciones Ópticas (CONICET La Plata-CIC), PO Box 3, (1897) Gonnet, Argentina
[4] Departamento de Ciencias Básicas, Facultad de Ingeniería, Universidad Nacional de La Plata, La Plata, Argentina

E-mail: edgar.rueda@udea.edu.co and amayad@ciop.unlp.edu.ar

CrossMark

Abstract

In this work a virtual 2f multiplexing system was implemented in combination with digital image compression techniques and redundant information elimination. Depending on the image type to be multiplexed, a memory-usage saving of as much as 99% was obtained. The feasibility of the system was tested using three types of images, binary characters, QR codes, and grey level images. A multiplexing step was implemented digitally, while a demultiplexing step was implemented in a virtual 2f optical setup following real experimental parameters. To avoid cross-talk noise, each image was codified with a specially designed phase diffraction carrier that would allow the separation and relocation of the multiplexed images on the observation plane by simple light propagation. A description of the system is presented together with simulations that corroborate the method. The present work may allow future experimental implementations that will make use of all the parallel processing capabilities of optical systems.

Keywords: optical diffraction, optical processors, optical multiplexing, image compression

(Some figures may appear in colour only in the online journal)

1. Introduction

Multiplexing and parallel processing are relevant in data transmission, processing, and storage applications. For instance in telecommunications, data multiplexing allows parallel transmission of several signals through one single channel; without data multiplexing, only one signal can be transmitted per channel [1–3]. In data storage applications, data multiplexing permits higher information storage using less storage memory [4–6]. Moreover, when parallel processing is implemented, processing times are reduced significantly [7]. In this sense, optical systems allowed fast parallel processing and multiplexing of information in 2D arrangements, which will be called 'images' henceforth. On the one hand, parallel processing can be achieved by simple light propagation through an optical setup, in principle at the speed of light. On the other hand, optical multiplexing uses light-wave superposition properties to pack several images within a single one. Another important feature of optical systems is the possibility of implementing digital processing techniques using digital cameras, spatial light modulators, and computer systems for the creation of opto-digital setups [8–12]. In this context, digital image compression techniques such as image spectrum processing [13–15], scalar quantization and compressive discretization [16] can be used to enhance optical multiplexing and encryption techniques proposed in opto-digital setups and virtual optical setups. In particular, Cabezas *et al* [17] proposed a virtual optical method named optical smart packaging (OSP), which reduces the amount of memory space used by several images that need to be stored or transmitted. Based on an optical multiplexing scheme, this method is intended to be an alternative to the existing digital-compression techniques. In this method, first a random phase mask multiplies the image that will be multiplexed, and then it is Fourier transformed using a virtual optical 2f scheme. The random phase mask distributes evenly

the energy over the Fourier plane. Next, the Fourier transformed complex-image is multiplied by a sinusoidal amplitude grating assigned to the image, and it is added to the other processed complex-images, forming the multiplexed OSP. This multiplexed complex-image package only carries amplitude and phase information corresponding to one image regardless of the amount of multiplexed images. To recover a particular image, the OSP is Fourier transformed in a virtual optical 2f scheme, obtaining pairs of all the multiplexed images separated in space at the exit plane. This allows a filtering procedure to ultimately obtain the image of interest. Although Cabezas *et al* [17] reported that this technique led to high storage capacity with no cross-talk noise, which is of great relevance for information transmission and storage for different reasons, they do not make use of the virtual optical 2f scheme at its full capacity. First, while using a random phase mask, the complete Fourier plane must be stored in order to avoid random information loss. Secondly, using amplitude sinusoidal gratings leads to images that will be replicated at the exit plane in the demultiplexing step while most of the energy goes to the zero diffraction order; this reduces both the efficiency of the system and the available storage space. Finally, the technique is designed to recover all images at once. If users are interested in a specific image, they would have to scan the exit plane to find it, which constitutes a problem when considering a real optical 2f demultiplexing scheme. To make use of the full capacity of the virtual optical 2f scheme, the current work eliminates the random phase mask, and compensates the concentration of the energy at the centre of the Fourier plane through a nonlinear scalar quantization technique. Because the energy is concentrated at the centre and the input image is real-valued, we used compressive discretization and redundant information elimination principles. In this way, storing the complete Fourier plane was unnecessary and helped to reduce the data needed to either store or transmit the information. In this work, we also replace the sinusoidal gratings by phase diffraction carriers that we have dubbed the image-positioning key (IPK). This contributed to eliminating both image replicas and the zero diffraction order at the exit plane. This increased the multiplexing capacity, the system efficiency and allowed positioning the image of interest at the centre of the exit plane.

2. Method description

The main goal of optical image multiplexing techniques is the optimization of image storage and transmission. This is achieved by overlapping the images in a two dimensional space array that requires less space than the sum of the individual images. In particular, to achieve these goals we have first performed on each image in the multiplexing step a digital Fourier transform (FT), followed by the multiplication of an image-positioning key (IPK) in order to avoid crosstalk. Next, the resulting complex data images are added into a 2D array we have dubbed the complex data package (CDP). Finally, we have applied digital-compression techniques eliminating redundant information for reducing the amount of

data required to represent, store, and transmit the CDP, while maintaining a defined minimum and acceptable standard of image quality. Because the main goal of this present work is based on the reduction of the amount of data required for the CDP, in the first part of this section we characterize the Fourier optical spectrum of individual images considering the effective bandwidth that encompasses the most significant frequencies, the symmetries of their Fourier spectrum (FS), and the optimal quantization of the amplitude and phase levels. In the second part of this section we will describe the multiplexing technique, which is based on the implementation of IPKs.

2.1. Compression of the image spectrum

In order to use the minimum amount of data to store an image while preserving the most relevant information of the (FS), we have studied three representative types of image on account of their spectral composition, purpose, and final use. The first type of image is binary characters (figure 1(a)); they are extensively used in written communication, easily recognizable by human inspection, and machine pattern-recognition algorithms due to high data redundancy, tolerating an important loss of frequency information. The second type is quick response (QR) codes (figure 1(b)); they are designed to be read by commercial applications without quality loss of the embedded data even in the presence of noise or code damage. This implies that an important loss of frequency information is acceptable, although not as high as in the case of the binary characters. The last type is 256-grey level images (figure 1(c)); in contrast to binary characters and QR codes, they can only tolerate a minimum loss of frequency information before degradation becomes perceptible by human observers.

Each image is represented by the one-dimensional function g, and its FS by G, where

$$G(\nu) = \int g(x) \exp(-i2\pi x\nu)dx, \tag{1}$$

x is the spatial-coordinate, and ν is the frequency-coordinate. As is well known, by inverse Fourier transforming G the original, image g can be recovered. However, although the complete FS is necessary to recover the original image, storing the complete spectrum is unnecessary when certain image quality loss is acceptable. In order to select the relevant information for each image spectrum, three aspects are analysed in the complex field G: low-pass filtering, redundant information removal, and quantization. This yields a new spectrum $\hat{G}$ that corresponds to a new image $\hat{g}$. Differences between image $\hat{g}$ and image g for each type of image will be evaluated in the following subsections.

2.1.1. Effective bandwidth.
An established criterion for the effective bandwidth is to include 98% of the total spectral power contained in G [18, 19]. However, our interest focuses on determining an effective bandwidth that takes into account the final purpose of the image g. For example, figure 2 shows that the character G is recognizable after filtering 15% of its
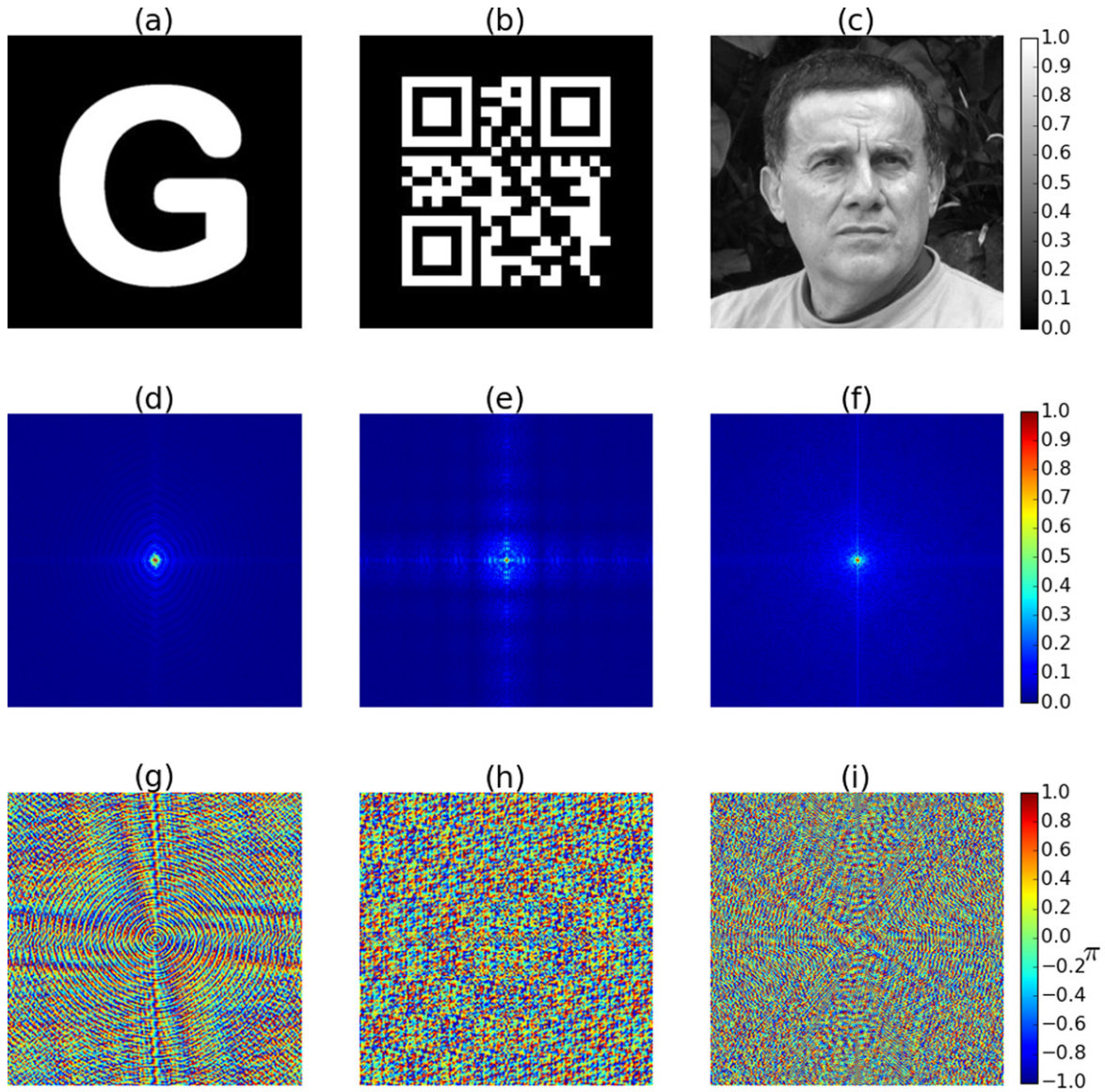
Figure 1. Image types and their corresponding FS. (a) Binary character, (b) QR code, (c) 256-grey level image. FS amplitude of (d) binary character, (e) QR code, and (f) 256-grey level image. FS phase argument of (g) binary character, (h) QR code, and (i) 256-grey level image. (d)–(i) A jet-colormap is used for facilitating visualization.
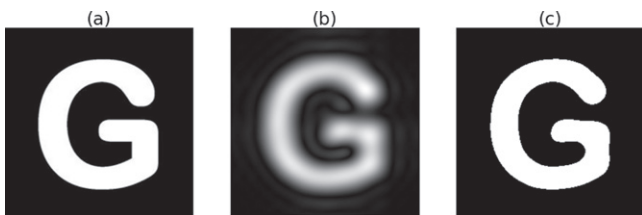

Figure 2. (a) Original image of character G, (b) recovered dynamic range adjusted image with 85% of the energy (5% of the Fourier plane side-length) after filtering with a LPF, (c) binarized recovered image.

energy with a low-pass filter (LPF), which is below the maximum percentage suggested by the established criterion. For this reason we are seeking an effective bandwidth for each type of image using a quality criterion and taking into account the final purpose of the recovered image. In order to

find each effective bandwidth, an image quality assessment based on the correlation coefficient (cc) is used. The cc is defined as:

$$cc = \frac{\sum_{n,m}(g_{n,m} - \bar{g})(\hat{g}_{n,m} - \bar{\hat{g}})}{\sqrt{\sum_{n,m}(g_{n,m} - \bar{g})^2 \sum_{n,m}(\hat{g}_{n,m} - \bar{\hat{g}})^2}} \qquad (2)$$

where n and m correspond to the pixel position in the 2D array, and $\bar{g}$ and $\bar{\hat{g}}$ correspond to the mean pixel value of the original and recovered image, respectively. To find the effective bandwidth of a representative image g (for each type of image), an FT is performed and a fraction-square area of the spectrum is extracted by using a LPF centred at the origin. This procedure will conserved only a percentage of the central part of the Fourier plane (FP). This fraction of the FP is inverse Fourier transformed into a fully recovered new image $\hat{g}$. Thus the cc with respect to the original representative
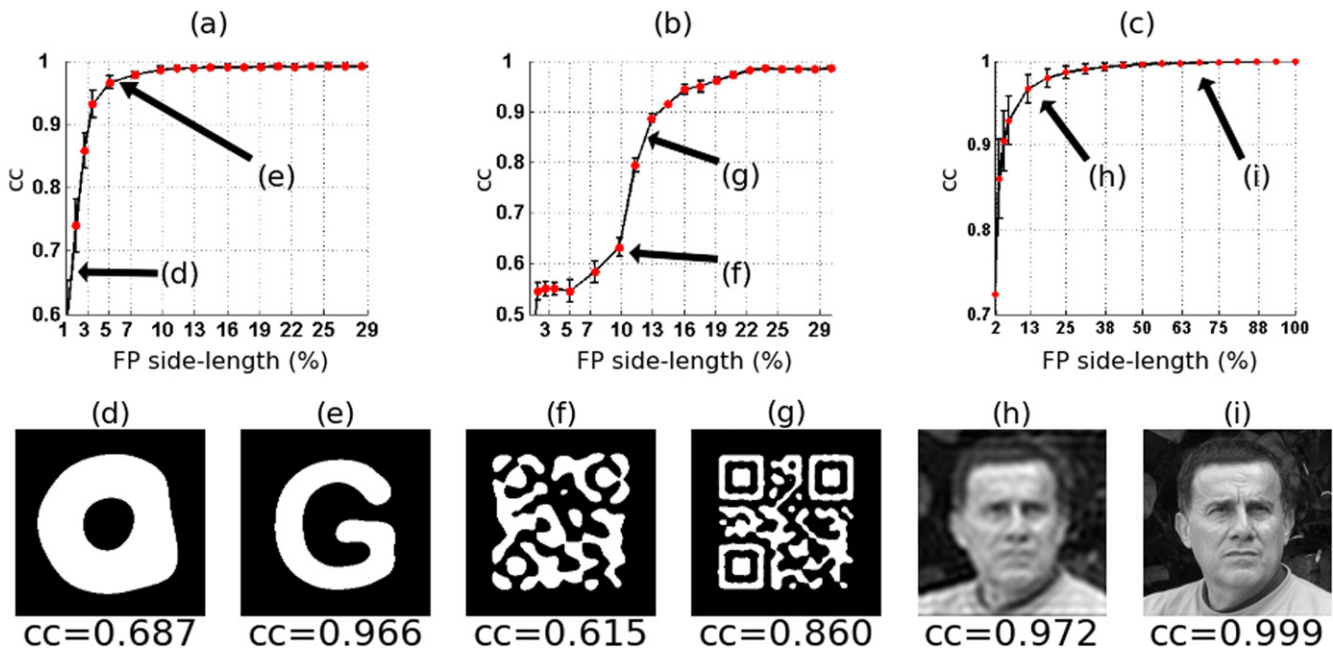
Figure 3. Average cc values for different FP side-length percentages. (a) Binary character G, (b) QR code, and (c) 256-grey level image. Images of the recovered binary character G with a FP side-length of (d) 2% and (e) 5%, and for a QR code with a FP side-length of (f) 7% and (g) 13%, and for a 256-grey level image with a FP side-length of (h) 13% and (i) 70%.

image is determined. The aforementioned procedure is repeated for increasing FP percentages until a minimum acceptable image quality is achieved, with an associated minimum image quality cc value. The minimum acceptable image quality is chosen for each type of image depending on its final purpose.

To generalize this result for each type of image, the procedure described above was implemented on a sample of 81 images, obtaining an average minimum image quality cc value (see figure 3). It is worth mentioning that this average value will correspond to the lowest Fourier plane percentage (LFPP) for each type of image.

For the case of binary characters, the LFPP corresponds to a situation where the character is recognizable, a low quality character (LQC). It is important to note that although LQCs are recognizable, they have an important high-frequency loss, which leads to severe loss of visual detail. When detail is of great importance high frequencies cannot be filtered and the LFPP will correspond to the situation where any quality loss is imperceptible by humans; this type of image will be called high-quality character (HQC). For the image type corresponding to QR codes, the LFPP is chosen based on the capability of the QR to be read by a commercial QR code reader. Finally, for 256-grey level images, the LFPP should correspond to a situation where no damage to the original image is perceptible by human visual inspection.

2.1.2. Symmetry. 2D FTs have Hermitian symmetries when the original image is real-valued [20, 21]. As shown in figure 4, the FT of the image under an inversion with respect to its origin has even parity for amplitude and odd parity for phase (quadrants I and III, and II and IV) [22]. Thus, in order to preserve and store the relevant information of the image
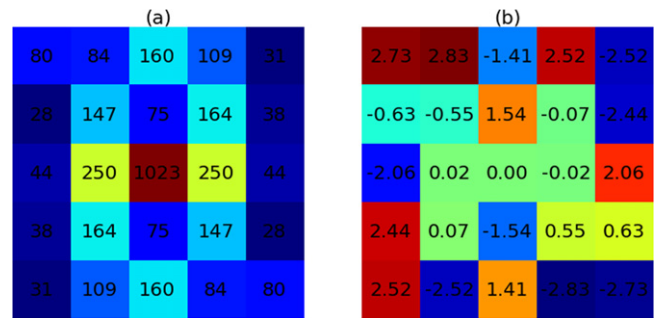

Figure 4. Central part of the FS of the image in figure 1(c). (a) 10 bit dynamic range amplitude, and (b) phase argument in radians. A jet-colormap is used to facilitate visualization.

FS, only quadrants I and II, or III and IV have to be stored. For example, to recover the image spectrum the information of quadrants III and IV will be obtained from quadrants I and II. This procedure allows 50% memory saving by removing all redundant information without losing spectral information.

2.1.3. Quantization of the amplitude and phase levels. So far it is evident that the whole spectrum is unnecessary to recover an image with a minimum acceptable quality. We will now cover separately the quantization of amplitude and phase of the complex spectrum. Quantization implies choosing a finite dynamic range from the entire range of the continuous signal and dividing it into quantization intervals. Then, the values of the continuous signal, encompassed within a certain quantization interval, are replaced by a single representative value (ith quantization level). As the differences between the continuous signal values and their corresponding quantization levels introduce quantization errors, they will be evaluated
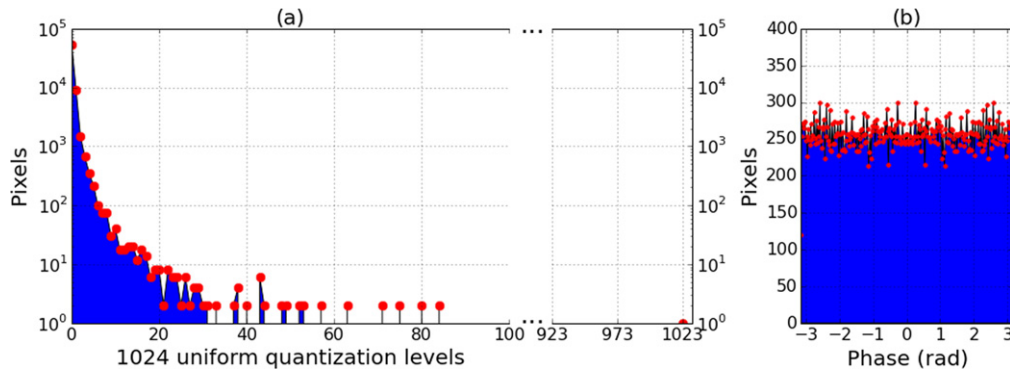
Figure 5. Histogram of the FS of the image in figure 1(c). (a) Amplitude, and (b) phase argument.

using the cc between the image recovered from the quantized spectrum and the original image. It is worth highlighting that the selection of the quantization intervals and the single representative values depends on the accuracy requirements of the signal-quantized representation. Thus, bearing in mind that the goal of this work is to store the least amount of spectral information needed to retrieve the image with a minimum acceptable quality, an optimized quantization process will be implemented in order to reduce the number of bits needed to represent the complex spectrum.

Because the general form of phase distribution probability of the images studied corresponds to a uniform distribution (see figure 5(b)), an optimal choice for quantization is uniform quantization. Uniform quantization divides the dynamic range into equally spaced quantization intervals and assigns a single representative value to each interval. To show the effect of a uniform phase quantization, we recovered the image of figure 1(c) after quantizing its phase spectrum with 4, 8, and 32 uniform quantization intervals, while keeping the full amplitude of the spectrum. The results can be seen in figure 6: 32 phase quantization intervals have been necessary to recover the image with a minimum acceptable quality.

In the case of the amplitude of the spectrum, its amplitude distribution of probability is not uniform. Its spectrum is concentrated around the lower amplitude values, followed by a gap without information, wherein a few values concentrate around the highest amplitude value (see figure 5(a)). For instance, when a uniform amplitude quantization of 1024 quantization intervals is applied to the spectrum of the image in figure 1(c), only 64 of the 1024 intervals contain information due to the gap in the amplitude probability distribution (see figure 7(a)). Because the information at the highest amplitude value is of great importance to recover an image with an acceptable minimum quality, a non-uniform amplitude quantization is needed using the minimum amount of quantization intervals.

We have chosen a non-uniform quantization technique known as a compression-expander [23], which compresses firstly the dynamic range of data using a nonlinear transformation, and then applies a uniform quantization to the transformed data. After applying different transformations, it was found that, for the specific type of information
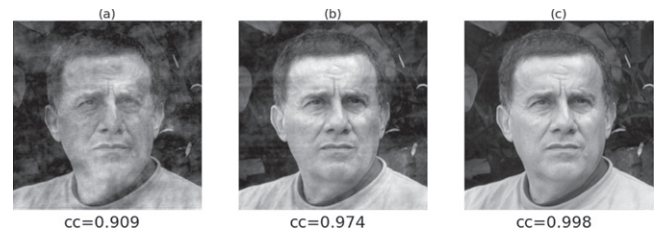

Figure 6. Images recovered after uniform phase quantization of the spectral information of the image in figure 1(c), conserving the full amplitude information of the spectrum. Each image was quantized with (a) 4, (b) 8, and (c) 32 uniform phase quantization levels corresponding to 2, 3, and 5 bits, respectively.

we are quantizing, the most effective method is a logarithmic transformation (see figures 7(b) and 7(c)).

To recover the original information, the inverse of the logarithmic transformation has to be applied (figure 7(d)). To show the effect of a non-uniform amplitude quantization, we recovered the image of figure 1(c) after applying the compression-expander technique with 4, 8, and 64 uniform amplitude quantization intervals, while keeping the full phase information of the spectrum. The results of this procedure can be seen in figure 8: 64 amplitude quantization intervals were needed in order to recover the image with a minimum acceptable quality.

We conclude from these results that a non-uniform quantization technique permitted an important reduction in the number of uql required to store the information of the amplitude spectrum. In contrast, for the case of the phase information of the spectrum, the non-uniform quantization was unnecessary.

2.2. Image multiplexing: complex data package

In order to multiplex N images without cross-talk and making use of the full capacity of optical multiplexing and image compression techniques, five steps are defined and explained below.

2.2.1. Image preparation. To perform the multiplexing procedure without cross-talk, each image g_k is digitally
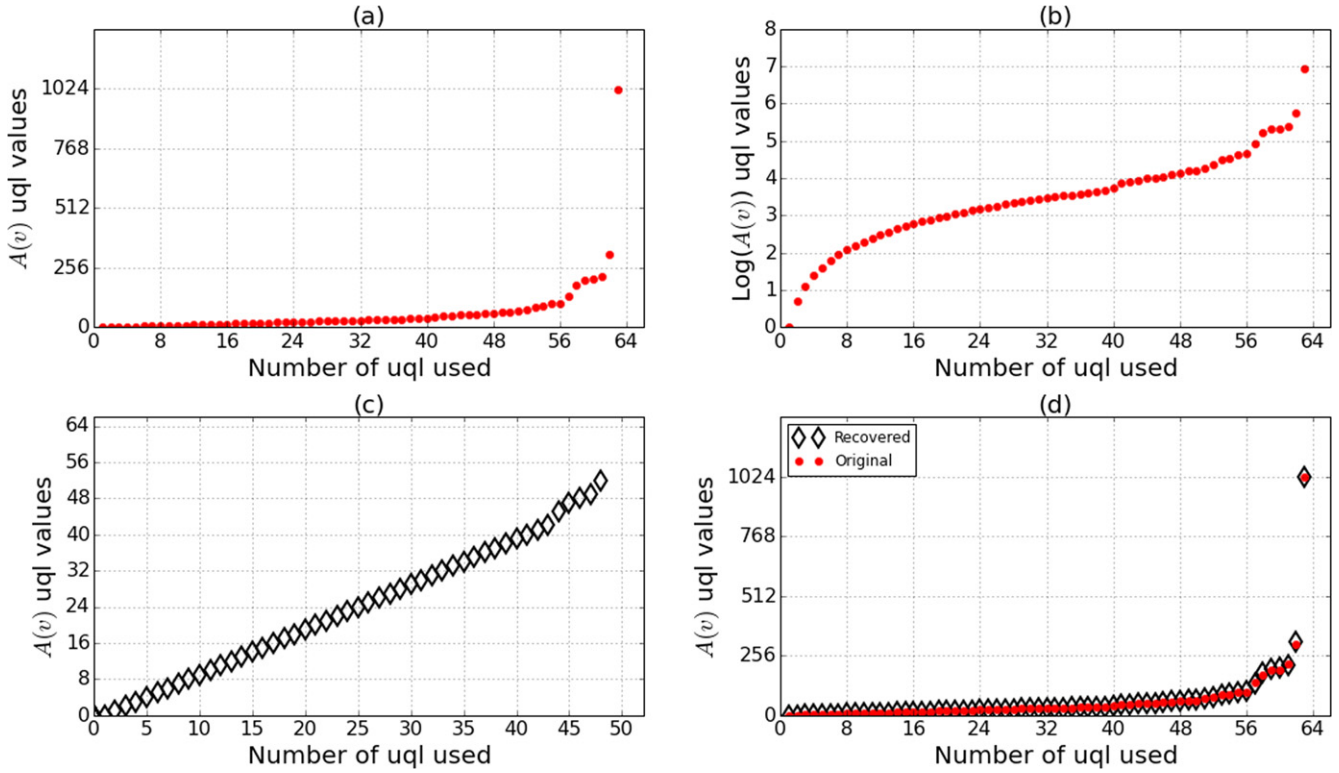
Figure 7. Quantization of the FS amplitude $A(v)$ of the image in figure 1(c). (a) Quantization of $A(v)$ using 1024 uniform quantization levels (uql). (b) Logarithm transformation of (a), $T(v) = Ln(A(v) + 1)$. (c) Quantization of normalized $T(v)$ using 64 uql. (d) Recovered $A(v)$ after applying the inverse transform $A(v) = \exp(T(v)) - 1$.
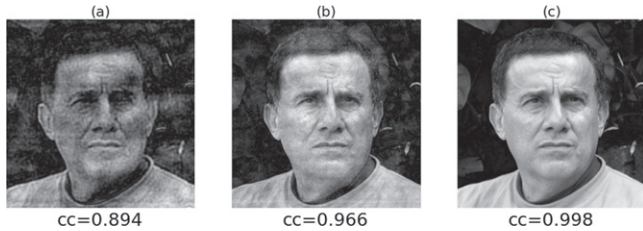

Figure 8. Images recovered after a non-uniform amplitude quantization of the spectral information of the image in figure 1(c) using the compression-expander technique, while conserving the full phase information of the spectrum. Each image was quantized with 4 (a), 8 (b) and 64 (c) uniform phase quantization levels corresponding to 2, 3 and 6 bits, respectively.

Fourier transformed and multiplied by an IPK,

$$P_k = FT\{g_k\}R_k = G_kR_k. \tag{3}$$

Here $FT\{\cdot\}$ is the FT operator and R_k is the IPK of the kth image. R_k is defined as

$$R_k(x, y) = \exp\left(-2\pi i a_k \frac{x}{\lambda z}\right)\exp\left(-2\pi i b_k \frac{y}{\lambda z}\right). \tag{4}$$

Coordinate (a_k, b_k) corresponds to the spatial position where the image will appear centred if an optical Fourier transform (OFT) is performed on P_k. In order to avoid cross-talk noise this coordinate must be determined correctly using

parameters such as image side-length, wavelength, and lens focal distance in order to avoid cross-talk noise at the exit plane. For the compression step, it is important to note that the arguments of each exponential function in equation (4) correspond to an odd function, which means that R_k has odd parity under an inversion with respect to the centre.

2.2.2. Digital multiplexing. After having prepared each image, the multiplexing is achieved by adding the N P_k complex-images, thus forming a new complex-image M,

$$M = \sum_{k=1}^{N}P_k. \tag{5}$$

M is a CDP that contains codified information of all the multiplexed images. To store the information content in M using an image format, two images are necessary: one for the amplitude information and one for the phase argument information.

2.2.3. CDP compression. Because the CDP is also a complex-image, all the three image compression techniques described in subsection 2.1 can be used. Firstly, the CDP is filtered using the LFPP for the type of images multiplexed. Secondly, because the CDP corresponds to the superposition of FTs of real images multiplied each by an IPK, the CDP phase argument has odd parity and the amplitude has even parity under inversion with respect to the centre, which allows
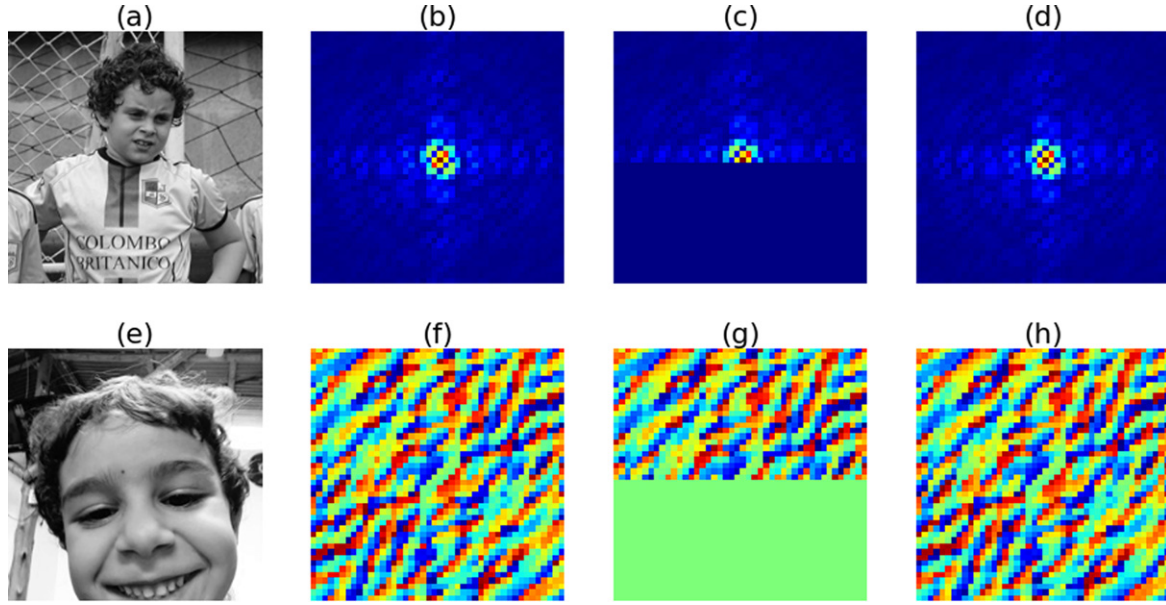
Figure 9. CDP symmetry under inversion about the centre. To show the symmetry, a CDP was created with images (a) and (e). (b) and (f) correspond to the amplitude and phase argument of the CDP; (c) and (g) are the stored amplitude and phase argument; (d) and (h) are the amplitude and phase argument recovered from the stored amplitude and phase argument (c) and (g), respectively. Images (b), (c), (d), (f), (g), and (h) are presented using a jet-colormap to facilitate visualization.

us to perform the same elimination of redundant information by storing only quadrants I and II of the original CDP (see figure 9 and appendix A). Thirdly, quantization of the CDP is performed by reducing the number of values (amplitude and phase levels) required to represent the 2D arrangement. Finally, the resulting CDP amplitude and phase argument are stored separately.

2.2.4. Demultiplexing. To demultiplex the images, the original CDP is rebuilt obtaining quadrants III and IV from quadrants I and II of the stored amplitude and phase argument (see figure 9). After rebuilding the original CDP, a specific image g_k is recovered by optically Fourier transforming the product between M and the complex conjugate of the IPK associated to image g_k,

$$S = MR_k^*$$ (6)

$$S = FT\{g_k\} + \sum_{\substack{l=1 \\ l \neq k}}^{N} FT\{g_l\}R_{lk},$$ (7)

where

$$R_{lk} = \exp\left(-2\pi i(a_l - a_k)\frac{x}{\lambda z}\right)\exp$$
$$\times \left(-2\pi i(b_l - b_k)\frac{y}{\lambda z}\right),$$ (8)

and applying an OFT $OFT\{\cdot\}$,

$$L = OFT\{FT\{g_k\}\} + \sum_{\substack{l=1 \\ l \neq k}}^{N} OFT\{FT\{g_l\}R_{lk}\},$$ (9)

$$L \approx g_k \otimes \delta(x, y) + \sum_{\substack{l=1 \\ l \neq k}}^{N} g_l \otimes \delta$$
$$\times (x - (a_l - a_k), y - (b_l - b_k)),$$ (10)

where $\otimes$ is the convolution process. This procedure guarantees that image g_k will be recovered and centred at coordinates $(0, 0)$ of the exit plane, while the remainder of the images will be centred at coordinates $(a_l - a_k, b_l - b_k)$. This avoids any unwanted cross-talk noise. The first term in (10) corresponds to the chosen image located at the centre of the exit plane, while the second term corresponds to the rest of the demultiplexed images located outside the centre of the exit plane. In the case of an optical demultiplexing system, the digital camera will only record the light at the centre of the exit plane (see figure 10). Thus, only the square module of the first term in equation (10) will be recovered and will correspond to the image chosen.

It is important to note that the CDP size depends on two main factors: the number of images to be multiplexed, and the percentage of the FP that is used depending on the type of image that was multiplexed. Thus, when multiplexing N QR codes with side-length n and a FP percentage FP%, the side-length of the CDP will be

$$n_{CDP} = FP\% \cdot n \cdot \sqrt{N}.$$ (11)

For example, with a CDP of 81 multiplexed images of side-length 256 pixels and a FP% of 13%, the CDP side-length is $n_{CDP} = 0.13 \times 256\sqrt{81} = 0.13 \times 2\,304 = 299$ pixels. In addition, if the symmetries are used (see subsubsection 2.1.2), the CDP image of 299×299 pixels will have, in fact, 299×150 pixels, which represents one half of the original size.
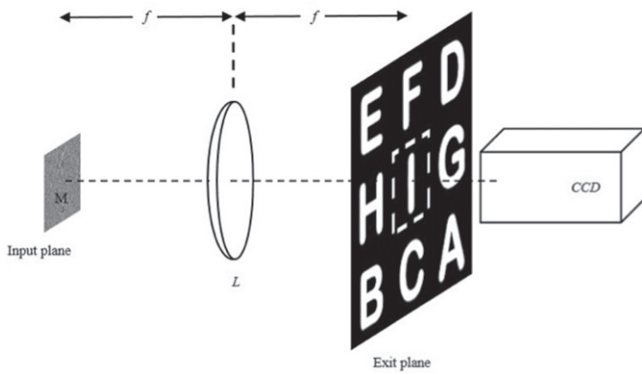
7

Figure 10. Optical-setup for the demultiplexing step. The complex-image S is projected and illuminated with a collimated beam-wave at the input plane. The resulting image is observed at the exit plane with a camera where only the information inside the dashed line box is stored.

Another important point is related to the correct generation of the IPKs. In order to build them with the appropriate frequency for the virtual and real demultiplexing steps, in such a way that the spatial positions where the images will appear do not generate any cross-talk, the original image must be embedded before applying the digital FT in an arrangement of zeroes with the size of the original CDP. An alternative solution would be to FT the image using its original size, and then rescale its FS up to a correct size, despite the introduction of noise produced by the rescaling algorithm.

3. Results

This section presents results on the application of the compression techniques for each type of image. These results comprise the number of levels, bit depth, and percentage of the FP that were employed to obtain the maximum memory savings while keeping the minimum acceptable quality for a single image spectrum and for a CDP of 81 multiplexed images (see figures 11 and 12). We also perform a test with a CDP of 529 images obtaining the same results as in tests for 81 images).

Tables 1 and 2 present results for the case of a single image spectrum and a CDP of 81 multiplexed images, respectively. From row two to row five, the results for each type of image are presented.

In both tables, columns two and three show the number of levels, and the corresponding bit depth, needed to store the quantized phase (PQ) and the quantized amplitude (AQ), respectively. In column four, the FP side-length percentage of the complex field is shown. In column five an example of the final size of the amplitude and phase images of a complex field of size 256×256 pixels is presented ($2\,304 \times 2\,304$ pixels for the CDP). In columns six and seven the weight of the original and after-compression images are given, respectively. Column eight contains the total percentage of memory savings. The recovered images of tables 1 and 2 can be seen in figure 11.

Figure 12 displays the exit planes obtained from CDPs with 81 multiplexed images for the three types of images. For the case of binary characters, the HQC case alone is presented. The red line box highlights the images that are shown in figures 11(j), (k) and (l).

Experimental parameters for the case of 81 HQC images were obtained considering a digital multiplexing step and a demultiplexing step in a virtual optical setup. For storage or transmission purposes, the CDP had 461×230 pixels, the CDP phase image had 5 bits and the amplitude image had 4 bits. For the demultiplexing step in a virtual optical setup, the CDP had 461×461 pixels, the phase image had 5 bits and the amplitude image had 8 bits after the inverse non-uniform quantization. The CDP display system in the optical setup had a 8.7 μm pixel size of and a resolution of at least 461×461 pixels. The 2f optical setup had a lens of 30 cm of focal length, a wavelength of 532 nm, and a camera with a maximum pixel size of 8.7 μm. For this configuration the IPKs had a minimum period of 18 μm and a maximum of 72 μm. The exit plane had an area of 19.92 mm $\times$ 19.92 mm and each image had a side-length of 2.22 mm. It is important to note that for the virtual optical demultiplexing step the CDP was embedded in an arrangement of $2\,304 \times 2\,304$ pixels in order to generate the complete exit plane space. By contrast, in a real optical setup the CDP would not have to be embedded, having a size of 461×461 pixels.

4. Discussion

Based on the results shown in tables 1 and 2, it was concluded that the effective bandwidth of the 256-grey level images is 3.5 times greater than the effective bandwidth of the HQCs, which is the largest one among the binary images studied. This great difference is mainly due to the purpose of each type of image, where the 256-grey image does not tolerate an important loss of high frequencies. This can be clearly seen in figure 3(g). Here, although the 256-grey level image with an FP% of 13% does not reach the minimum image quality, the binary images reach it with an equal FP% for the QR code and a lower FP% for the LQC (figures 3(d) and (f)). For the case of quantization of amplitude and phase levels, 256-grey level images need levels four times higher than binary images, which share the same phase number and amplitude quantization levels. This could be explained by the dependence of the dynamic range on the bandwidth, the energy difference between the zero order (almost the double for 256-grey level images), and the higher frequencies. In column five, the symmetries used allowed for a reduction of the image spectrum size by a factor of two. The percentage of savings in column eight was calculated using columns six and seven. Original binary images have a 1-bit pixel depth, while 256-grey level images have an 8 bit pixel depth. It is worth noting that the savings percentages in table 2 were obtained by applying directly the quantization levels and FP% of table 1 to the CDPs. These percentages are equal, as it can be appreciated when comparing column eight of both tables. This means that the characterization of a single image
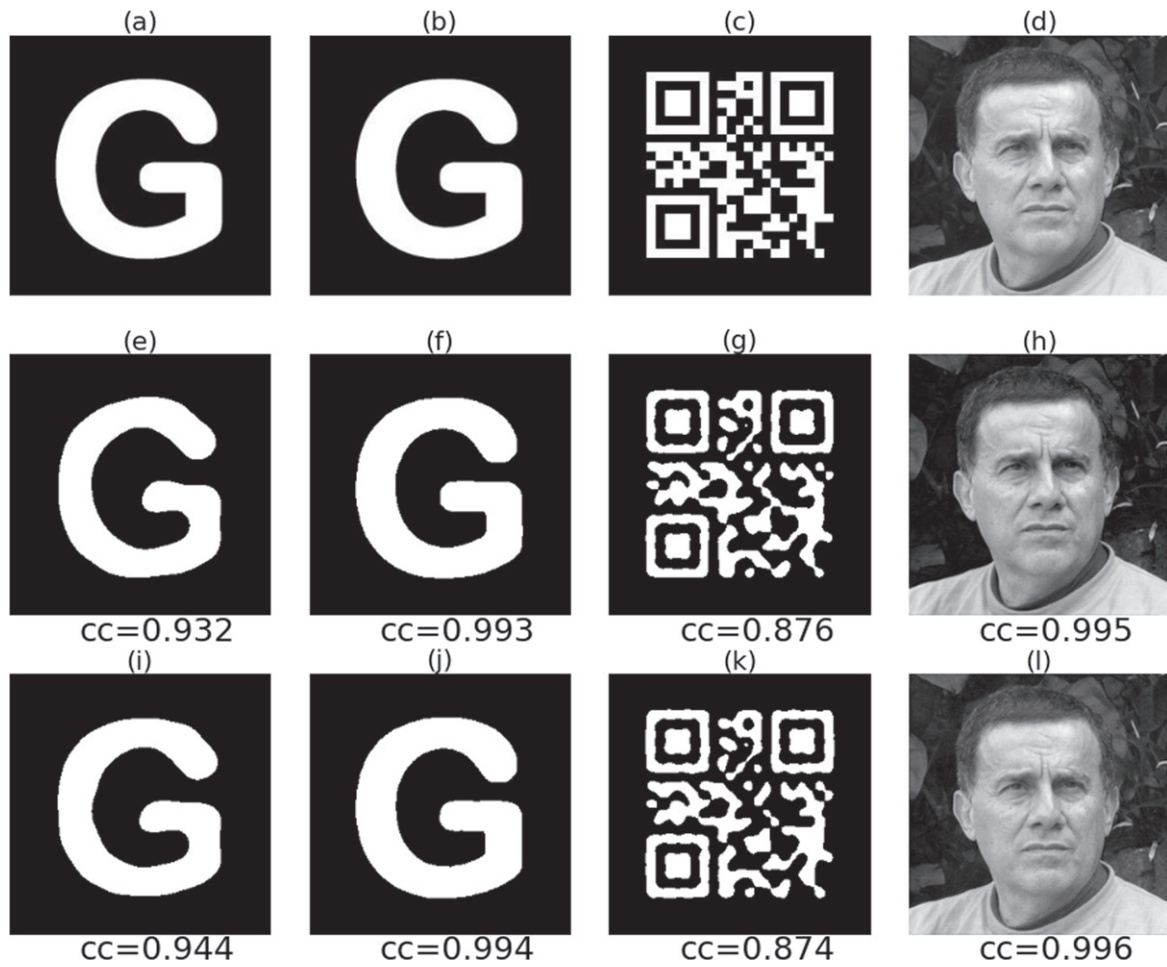
Figure 11. Recovered images after applying the three compression techniques: LPF, phase argument quantization (PQ) and amplitude quantization (AQ), and FP redundant information elimination. Images (e) to (h) correspond to the case of a single image. Images (i) to (l) correspond to the case of a CDP of 81 multiplexed images. (a) and (b) are the original binary character G, (c) original QR code, and (d) original 256-grey level image. (e) and (i): Recovered LQC with FP% = 5%, PQ = 32 bit, and AQ = 16 bit, for a total saving of 99%. (f) and (j): Recovered HQC with FP% = 20%, PQ = 32 bit, and AQ = 16 bit, for a total saving of 82%. (g) and (k): Recovered QR code with FP% = 13%, PQ = 32 bit, and AQ = 16, for a total saving of 92%. (h) and (l) Recovered 256-grey level image with FP% = 70%, PQ = 32 bit, and AQ = 64 bit, for a total saving of 66%.
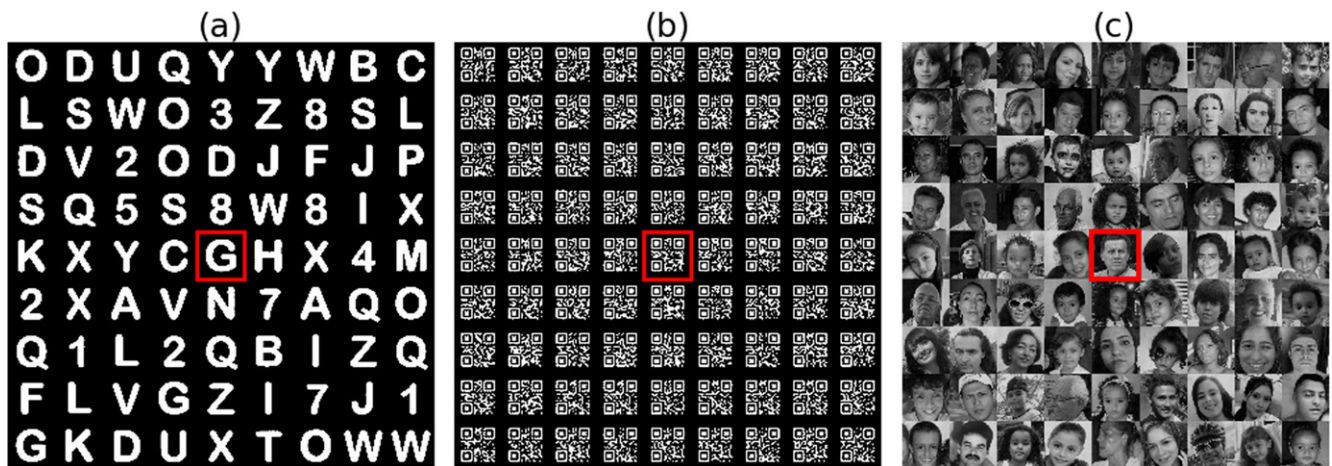

Figure 12. Recovered images at the exit plane from the CDP with 81 multiplexed images. (a) HQC images, (b) QR codes, and (c) 256-grey level images.

10

Table 1. Single image spectrum compression results.

Case recovered image	PQ number of levels/ bit depth (bit)	AQ number of levels/ bit depth (bit)	FP% (complex field)	Amplitude and phase image size for 256×256 complex field (pixel)	Original weight (bit)	After compression weight (bit)	% saving
HQC	32/5	16/4	20%	51×26	65 536	11 934	82%
LQC	32/5	16/4	5%	13×7	65 536	819	99%
QR code	32/5	16/4	13%	17×33	65 536	5049	92%
256-grey level	32/5	64/6	70%	179×90	524 288	177 210	66%

Table 2. 81 multiplexed images CDP compression results.

Case recovered image	PQ number of levels/bit depth (bit)	AQ number of levels/bit depth (bit)	FP% (complex field)	Amplitude and phase image size for 2 304 × 2 304 complex field (pixel)	Original weight (bit)	After compression weight (bit)	% saving
HQC	32/5	16/4	20%	461 × 231	5308 416	958 419	82%
LQC	32/5	16/4	5%	115 × 58	5308 416	60 030	99%
QR code	32/5	16/4	13%	299 × 150	5308 416	403 650	92%
256-grey level	32/5	64/6	70%	1613 × 807	42 467 328	14 318 601	66%

spectrum allows for the prediction of the parameters and savings percentage for a CDP of any number of multiplexed images of the same type. Comparing the percentage of savings of the binary images evinces that smaller effective bandwidths allow for greater savings.

5. Conclusions

We have applied digital-compression techniques that have eliminated redundant information for reducing the amount of data required to represent, store, and transmit a complex data package (CDP), while maintaining a minimum acceptable image quality for three types of images: binary characters, QR codes, and 256-grey level images. We made a characterization of the Fourier optical spectrum of individual images by studying the effective bandwidth that encompasses the most significant frequencies, the symmetries of their Fourier spectrum, and the optimal quantization of the amplitude and phase levels. We found that LQC require the lowest effective bandwidth of all the image types studied, because all of the spectrum frequencies necessary for their recognition are close to the zero order. By contrast, for the 256-grey level images the highest bandwidth was required, as high frequencies are important for reaching the minimum acceptable quality for this kind of image. Since the original images had only real information, their complex spectrums had symmetries that allowed us to eliminate half of the spectrum data without losing information. Similarly, in this work we demonstrated that these symmetries are conserved for the CDPs, which allowed the elimination of half the CDP data without losing information on the package. We also concluded that since the values of phase of the spectrums are uniformly distributed a uniform quantization was the most adequate. For the case of the amplitude, since its values are highly localized great dynamical ranges have to be used in order to keep all the important information of the spectrum, thus making necessary the use of non-uniform quantization levels. For the amplitude, a non-uniform quantization of logarithmic type was used to be able to implement small dynamical ranges without losing information. All image types required 32 quantization levels for the phase, whereas for the amplitude, due to the high variations of the dynamic range, the 256-grey level images required four times more levels than the binary images. Combining the three compression strategies yielded important memory space savings percentages. In particular, 1-bit per pixel binary images reached space saving percentages of around 99%, 92%, and 82%, for the LQC, QR code, and HQC, respectively. For the 256-grey level images, a 66% space saving is significant taking into account that a visual inspection does not provide appreciable information loss. A highly relevant result is the fact that space saving percentages were the same for a single image and for CDPs, regardless of the number of images multiplexed in the CDP. In particular, we corroborated the previous statement using 81 as well as 529 multiplexed images. In addition, the technique we presented here takes into account the experimental parameters, which are important for its compatibility with different opto-

digital encryption techniques. In fact, the FT of the first step could be performed optically if one recovers the complex field of the transformation, because all the digital processing is applied to the complex Fourier spectrum or CDP.

Appendix A. CDP even and odd parity conservation

By defining 1D odd and even functions, we demonstrate here that a CDP of real images has amplitude with even parity and phase argument with odd parity under a coordinate inversion, provided that each IPK phase argument has odd parity.

Defining even function $e(x)$ and odd function $o(x)$, where for $x \in \mathbb{R}$

$$
\begin{aligned}
e(-x) &= e(x) \\
o(-x) &= -o(x)
\end{aligned}
\tag{A.1}
$$

the following properties are satisfy:

1. $e(x)e(x)$ is an even function.
2. $o(x)o(x)$ is an even function.
3. $o(x)e(x)$ is an odd function.
4. $o(x) \pm o(x)$ is an odd function.
5. $e(x) \pm e(x)$ is an even function.
6. $e^n(x)$ with $n = 3, 4, 5 \ldots$, is an even function.
7. $o^n(x)$ with $n = 4, 6, 8, \ldots$, is an even function.
8. $o^n(x)$ with $n = 3, 5, 7, \ldots$, is an odd function.

If we expand cosine and sine functions in a Taylor expansion,

$$
\begin{aligned}
\cos(z) &= 1 - \frac{z^2}{2!} + \frac{z^4}{4!} - \ldots \\
\sin(z) &= z - \frac{z^3}{3!} + \frac{z^5}{5!} - \ldots
\end{aligned}
\tag{A.2}
$$

using the even–odd function properties it can be stated that

$$
\begin{aligned}
&\cos(e(x)) \text{ is an even function} \\
&\sin(e(x)) \text{ is an even function} \\
&\cos(o(x)) \text{ is an even function} \\
&\sin(o(x)) \text{ is an odd function.}
\end{aligned}
\tag{A.3}
$$

Next, defining a complex function $\varphi(x) = A(x)\exp(i\theta(x))$ there are only four possible combinations as shown in table A.1. Remembering that

Table A.1. Possible outcomes for the amplitude and phase argument of a complex function.

If $A(x)$ is even and $\theta(x)$ is odd:	If $A(x)$ is odd and $\theta(x)$ is even:
$\Re\{\varphi(x)\} = A(x)\cos(\theta(x))$ is even	$\Re\{\varphi(x)\} = A(x)\cos(\theta(x))$ is odd
$\Im\{\varphi(x)\} = A(x)\sin(\theta(x))$ is odd	$\Im\{\varphi(x)\} = A(x)\sin(\theta(x))$ is odd
If $A(x)$ is odd and $\theta(x)$ is odd:	If $A(x)$ is even and $\theta(x)$ is even:
$\Re\{\varphi(x)\} = A(x)\cos(\theta(x))$ is odd	$\Re\{\varphi(x)\} = A(x)\cos(\theta(x))$ is even
$\Im\{\varphi(x)\} = A(x)\sin(\theta(x))$ is even	$\Im\{\varphi(x)\} = A(x)\sin(\theta(x))$ is even

$G(\upsilon)$ is the FT of image $g(x)$, $G_1(x) = A_1(x)\exp(i\theta_1(x))$ and $G_2(x) = A_2(x)\exp(i\theta_2(x))$ will correspond to the FTs of real images $g_1(x)$ and $g_2(x)$, where A_1 and A_2 are even functions and θ_1 and θ_2 are odd functions. If for simplicity we construct a CDP by adding G_1 and G_2 with IPKs $B_1(x) = \exp(i\beta_1(x))$ and $B_2(x) = \exp(i\beta_2(x))$, where arguments $\beta_1(x)$ and $\beta_2(x)$ are odd functions, defining $\rho_m(x) = \theta_m(x) + \beta_m(x)$ for $m = 1, 2$, we can write

$$
\begin{aligned}
G(x) &= A(x)\exp(i\rho(x)) = G_1(x) + G_2(x) \\
&= A_1(x)\exp(i\rho_1(x)) + A_2(x)\exp(i\rho_2(x)) \\
&= A_1(x)\cos(\rho_1(x)) + iA_1(x)\sin(\rho_1(x)) \\
&\quad + A_2(x)\cos(\rho_2(x)) + iA_2(x)\sin(\rho_2(x)) \\
G(x) &= \{A_1(x)\cos(\rho_1(x)) + A_2(x)\cos(\rho_2(x))\} \\
&\quad + i\{A_1(x)\sin(\rho_1(x)) + A_2(x)\sin(\rho_2(x))\}.
\end{aligned}
\tag{A.4}
$$

Thus $\Re\{G(x)\}$ is even and $\Im\{G(x)\}$ is odd, and from table A.1 we can state that the amplitude $A(x)$ is an even function and the phase argument $\rho(x)$ is an odd function. We then conclude that in general a CDP of real images under coordinate inversion has amplitude with even parity and phase argument with odd parity.

References

[1] Chitode J S 2009 *Analog and Digital Communication Engineering* (Pune: Technical Publications)

[2] Bobrinev V, Son J, Jeon H and Lee S 1997 Two-dimensional spectral multiplexing method for direct image transmission through an optical fiber *Opt. Eng.* **36** 15–21

[3] Tai A 1983 Two-dimensional image transmission through a single optical fiber by wavelength-time multiplexing *Appl. Opt.* **22** 3826–32

[4] Tebaldi M, Toro L A, Lasprilla M and Bolognini N 1998 Image multiplexing by speckle in a BSO crystal *Opt. Commun.* **155** 342–50

[5] Meng X F, Cai L Z, Wang Y R, Yang X L, Xu X F, Dong G Y and Shen X X 2009 Digital image synthesis and multiple-image encryption based on parameter multiplexing and phase-shifting interferometry *Opt. Lasers Eng.* **47** 96–102

[6] Singh M, Kumar A and Singh K 2008 Multiplexing in optical encryption by using an aperture system and a rotating sandwich random phase diffuser in the Fourier plane *Opt. Lasers Eng.* **46** 243–51

[7] Yong-Liang X, Su X, Li S, Liu X and Zeng S 2011 Key rotation multiplexing for multiple-image optical encryption in the Fresnel domain *Opt. Laser Technol.* **43** 889–94

[8] Alfalou A and Alkholidi A 2005 Implementation of an all-optical image compression architecture based on Fourier transform which will be the core principle in the realisation of the DCT *Proc. SPIE* **5823** 183

[9] Alfalou A and Brosseau C 2015 *Recent Advances in Optical Image Processing: Progress in Optics* vol 60 chapter 2 (Amsterdam: Elsevier) pp 119–262

[10] Alfalou A and Brosseau C 2009 Optical image compression and encryption methods *Adv. Opt. Photonics* **1** 589

[11] Henao R, Rueda E, Barrera J and Torroba R 2010 Noise-free recovery of optodigital encrypted and multiplexed images *Opt. Lett.* **35** 333–5

[12] Barrera J F, Vélez A and Torroba R 2013 Experimental multiplexing protocol to encrypt messages of any length *J. Opt.* **15** 055404

[13] Alfalou A and Brosseau C 2010 Exploiting root-mean-square time-frequency structure for multiple-image optical compression and encryption *Opt. Lett.* **35** 1914–6

[14] Alfalou A, Elbouz M, Mansour A and Keryer G 2010 New spectral image compression method based on an optimal phase coding and the RMS duration principle *J. Opt.* **12** 115403

[15] Alfalou A, Mansour A, Elbouz M and Brosseau C 2011 Optical compression scheme to simultaneously multiplex and encode images *Optical and Digital Image Processing: Fundamentals and Applications* ed G Cristobal *et al* (Weinheim: Wiley-VCH Verlag) pp 463–83

[16] Yaroslavsky L P 2015 Compression, restoration, resampling, 'compressive sensing': fast transforms in digital imaging *J. Opt.* **17** 073001

[17] Cabezas L, Tebaldi M, Barrera J F, Bolognini N and Torroba R 2012 Optical smart packaging to reduce transmitted information *Opt. Express* **20** 158–63

[18] Goodman J W 2005 *Introduction to Fourier Optics* (Englewood, CO: Roberts and Company) section 2.4.2

[19] Voelz D G 2011 *Computational Fourier Optics: a MATLAB Tutorial* (Bellingham: SPIE Press) section 2.2

[20] Sezan M I and Stark H 1982 Image restoration by the method of convex projections: part 2-applications and numerical results *IEEE Trans. Med. Imaging* **MI-1** 95–101

[21] Sorensen H, Jones D, Heideman M and Burrus C 1987 Real-valued fast Fourier transform algorithms *IEEE Trans. Acoust.* **35** 849–63

[22] Ruiz B and Granieri S 2003 The parity function in optical waves propagation *Optik (Stuttg)* **114** 207–12

[23] Yaroslavsky L 2004 *Digital Holography and Digital Image Processing: Principles, Methods, Algorithms* (New York: Springer) section 3.6.1